Fusion Engineering and Design 193 (2023) 113647

Contents lists available at ScienceDirect

Fusion Engineering and Design

journal homepage: www.elsevier.com/locate/fusengdes

Plasma diagnostics using fast cameras at the GOLEM tokamak

S. Abbasi [a,*], J. Chlum [a], J. Mlynar [a], V. Svoboda [a], J. Svoboda [a,b], J. Brotankova [a]

[a] Faculty of Nuclear Sciences and Physical Engineering, Czech Technical University in Prague, Brehova 7, Prague 115 19, Czech Republic
[b] Institute of Plasma Physics of the Czech Academy of Sciences, Za Slovankou 1782/3, Prague 182 00, Czech Republic

ARTICLE INFO

Dataset link: http://golem.fjfi.cvut.cz/shots/39304/

Keywords:
Plasma radiation
Fast visible camera
Tomographic inversion

ABSTRACT

Tomographic inversion of radiation determines spatial distribution of tokamak plasma radiation sources using line integrated plasma projections data. For measurements of the projections, fast visible radiation matrix cameras became broadly applied on tokamaks in recent past. These novel cameras opened new possibilities in high temperature plasma studies.

The GOLEM tokamak of the Czech Technical University in Prague strives to implement up-to-date diagnostics with enhanced temporal and spatial resolution. Therefore, a novel diagnostic system of two crossed monochrome cameras Photron FASTCAM MINI UX50 was integrated into the GOLEM diagnostics. The proposed contribution will detail their novel port mounts (vertical and horizontal) at the GOLEM tokamak which have been designed so that additional optical measurements of the plasma core (e.g. plasma spectroscopy) is possible.

As the main purpose of this study, we shall focus in particular on the frame rate potential which is high enough to make detection and observation of highly transient phenomena in the GOLEM plasmas possible. Progress in solving specific challenges of the ill-conditioned tomographic inversion via the algorithm optimization and testing for the GOLEM tokamak will be presented together with the first tomographic results.

1. Introduction

Radiation intensity distribution in the plasma reveals valuable insight into power balance studies in magnetically confined plasmas such as in tokamaks [1,2] and stellarators [3]. Due to the contribution of the accumulation of impurities inside the tokamak plasma to the total amount of radiation, analyses of the radiation diagnostics data can yield information to identify the spatially varying impurity concentration [4] especially for high atomic number impurities. Monitoring and mitigation of the impurities' central accumulation in real-time is important due to the detrimental effect on the tokamak plasma performance [5]. As the plasma radiation leads to plasma energy loss, it carries unique information on development of MagnetoHydroDynamic (MHD) instabilities [6] or the energy, current and dynamics of runaway electrons (REs) in tokamaks [7,8].

Spatial properties of radiation emitted from the magnetically confined plasmas has been recorded with various tools. Some research has been conducted by a two-camera bolometer system in Wendelstein 7-X (W7-X) [9], Soft X-ray (SXR) diagnostic in the ASDEX Upgrade tokamak [10], and the COMPASS tokamak [11]. SXR data have been also routinely analysed at Joint European Torus (JET) [12], as well as its neutron emission data from the JET neutron profile monitor [13]. In this respect, potential of the Radial Neutron Camera (RNC) project for ITER has been already studied on simulated data [14].

Similarly, at small tokamaks, the visible-light cameras can be used to record the visible radiation emitted from the plasma edge due to the interaction of neutral particles flux from wall and the gas fuelling with plasma. For measurements of the projections, fast visible radiation matrix cameras have become broadly applied on tokamaks in the recent past. Actually, these novel cameras opened up new possibilities even in high temperature plasma studies [15,16].

The tomographic inversion is a standard method for reconstructing the two dimensional emissivity profiles of the plasma using line integrated plasma projections data. Considering the toroidal symmetry of the tokamak [17], the radiation characterization can be provided by the tomographic inversion performed over one poloidal cross section only. However, the data is usually spatially sparse due to the limited number of observations angles and also varying rapidly in time. This underlines the importance of the temporal and spatial resolution of the projection data and its geometric precision [18]. Besides the quality of the measurements, the inversion algorithm method also plays a major role in the accuracy and reliability of the tomographic inversion as an ill-posed problem. Moreover, in order to handle this issue,

* Corresponding author.
E-mail address: saraabbasi2@gmail.com (S. Abbasi).

https://doi.org/10.1016/j.fusengdes.2023.113647
Received 31 October 2022; Received in revised form 31 January 2023; Accepted 8 March 2023
Available online 23 March 2023

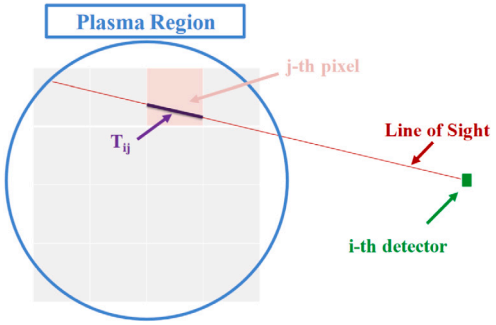

Fig. 1. Layout of discretization of a circular cross section of plasma region and the LoS of one detector in the tomographic system.

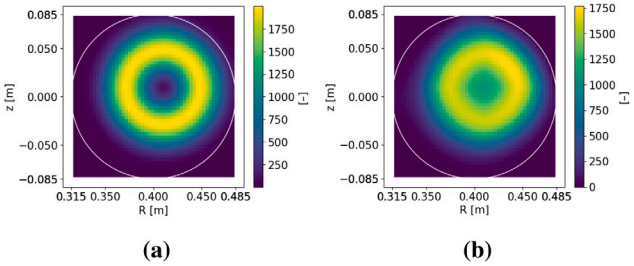

Fig. 2. (a) The artificial image of Phantom emissivity used for testing regularization method for the radial (R) and vertical (V) cameras layout (See Fig. 4(a)), and (b) Phantom inversion results obtained by using MFR with anisotropic smoothing algorithms. The light intensity (colorbar) is in arbitrary unit.

some a-priori information (constraints) is implemented by the applied regularization algorithms, in particular the expected smoothness of the emissivity [19]. Several techniques can be applied for solving the tomography problem, which specially focus on mitigating the influence of errors [10]. The Minimum Fisher Regularisation (MFR) based on the Tikhonov Regularization (TR) [20] is used as a method of tomography with an iterative optimization of the results within this contribution.

As the main purpose of this study, we focused in particular on the frame rate potential of the available hardware, which is high enough to allow detection and observation of highly transient phenomena in the GOLEM tokamak plasmas (see Section 4). Progress in solving specific challenges of the ill-conditioned tomographic inversion is performed using the MFR algorithm implemented in the Tomotok package [21] via the algorithm optimization and testing for the GOLEM tokamak together with the first tomographic results. Furthermore, perspectives of implementing further inversion constraints e.g. linked to integration of another visible light diagnostic data will be discussed.

This paper is organized as follows: Section 2 gives an overview of the Tomographic inversion, and Line of Sight (LoS) Layout. Section 3 implements a simple synthetic diagnostic model for testing the accuracy of the reconstruction result. Section 4 describes the system under investigation, the GOLEM tokamak with installed fast visible cameras. Section 5 details and discusses the reconstruction result provided by Tomotok package. Finally Section 6 presents a summary of the conclusions.

2. Tomographic inversion and line of sight layout

Tomographic inversion determines two dimensional emissivity profiles of plasma by using line integrated measurements acquired by detector–pinhole cameras observing the plasma. Toroidal symmetry is assumed in order to make conclusions about entire plasma volume from measurements in one poloidal cross section. Fig. 1 shows the layout of discretization of a plasma region and the LoS of one detector in the tomographic system in which the circular cross-section of the plasma region under investigation is discretized into N pixels. The spatial two-dimensional ($2D$) emissivity function g in the plasma region is discretized into the plasma emissivity distribution with value g_j in the j-th pixel of the tomographic reconstruction grid.

Each camera consists of a number of light intensity detectors whose fields of view together make up a fan of narrow cones. The simplest optical model for the camera setup is the pinhole chamber model. Considering smooth variation of the emission function over the view cones, each cone can be approximated by a single, zero-width LoS. Then, the measured signal intensity f_i corresponding to the incident light radiation on the i-ith detector is given by

$$\mathbf{f_i} = \sum_j \mathbf{T_{ij}}\ \mathbf{g_j}. \tag{1}$$

where T_{ij} is an element of the geometric matrix (also known as the response matrix) denoting the length of the ith LoS in the jth pixel, as depicted in Fig. 1. T_{ij} relates the weight of the radiation emitted from the plasma located in j-th pixel in the line integrated measurement of i-th detector. In order to reconstruct the unknown function g_j from the sparse measured signal f_i, the reconstruction matrix M_{ji} is introduced by some regularization methods (including, in particular, the MFR method),

$$\mathbf{g_j} = \sum_i \mathbf{M_{ji}}\ \mathbf{f_i}. \tag{2}$$

The reconstruction matrix usually addresses the ill-posedness of the inversion task and its underdetermination stemming from the limited number of detectors and viewing angles by implementing some prior information and constraints, in particular, some constraint on smoothness of the solution and/or information on the shape of the confining magnetic field. The Minimum Fisher Regularisation (MFR) algorithm is applied in order to increase weight of channels with higher signal intensity [18,22].

3. Accuracy tests

The data recorded via the diagnostic cameras are limited to a few poloidal angles, hence the signal data is considered sparse. In addition, the used inversion algorithm produces some errors in the reconstruction result. This makes it important to perform validation of the reliability and the accuracy of the reconstruction result [18]. In order to test the accuracy of the present work two following procedures are used:

(i) Test runs using phantom images: In this procedure a narrow Gaussian function is used to simulate a hollow emissivity profile as a model (phantom) image. The tomography algorithm is applied to calculate the line-integrated data corresponding to the phantom by considering the applied geometric matrix of reconstruction based on Eq. (1). Then the reconstructed image of this line-integrated data is compared with the model image (phantom). In order to produce a signal similar to the real signal from the cameras, a noise with a Gaussian distribution ($\mu = 0$, $\sigma = 3$) is added to the simulated signal. Fig. 2(a) shows (a) The artificial image of Phantom emissivity used for testing regularization method for the radial (R) and vertical (V) cameras layout (See Fig. 4(a)) and (b) Phantom inversion results obtained by using MFR with anisotropic smoothing algorithms. The inversions were performed on a square rectilinear grid of size 60 × 60 pixels with a total size of 17 cm ×17 cm. The grid size in discretization of the phantom image, the lines of sight layout to calculate the line integrated data corresponding to the phantom and consequently, the applied geometric matrix of reconstruction is identical to all applied studies of real data in the following sections. Therefore, the accuracy of the reconstruction result of the phantom image as a test can be used as a

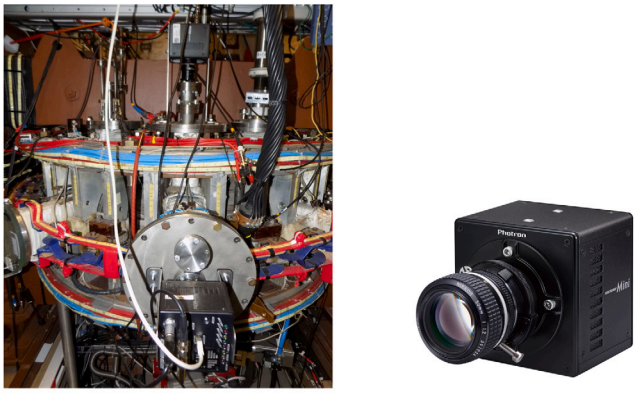

(a) (b)

Fig. 3. (a) The GOLEM tokamak with the installed R and V cameras, and (b) detail of the fast visible matrix camera, Photron FASTCAM MINI UX50.

relevant information of the accuracy of the reconstruction result of the real data. According to this comparison, it can be noticed that the cavity is less pronounced in the reconstructed profile than in the phantom profile. The reconstructed profile is also smoother. The reconstructed profile also has an overall more 'square' shape, rather than round which should arise even when performing tomography on real data.

(ii) Backfit of the reconstructed image: In this procedure the recorded line integrated signal acquired by two cameras is compared with the signal corresponding to the reconstructed result based on Eq. (1). This accuracy method will be used to test the reconstruction result presented in Section 5.

4. The GOLEM Tokamak with installed fast visible cameras

The GOLEM tokamak [23] of the Czech Technical University in Prague strives to implement up-to-date diagnostics with enhanced temporal and spatial resolution. The novel diagnostic system is composed of two crossed monochrome cameras Photron FASTCAM MINI UX50 placed in the same poloidal cross-section. The cameras are with a Maximum Frame Rate of 160,000 fps (1280 × 8 pixels) in 12-bit ADC dynamic range [24] with detector size 10 μm × 10 μm. The cameras observe light in the visible and near IR range with the highest response at 630nm. The cameras' spectral response curve is described in detail in [24].

Fig. 3(a) and Fig. 3(b) show, respectively, the GOLEM tokamak with the installed R and V cameras, and the fast visible camera, Photron FASTCAM MINI UX50. Furthermore, Fig. 4(a) shows the Schematic figure of the Poloidal GOLEM tokamak cross-section with the geometry of the lines of sight of two V and R fast visible cameras in respectively red and purple resulting in vertical and radial line integrated visible light data. Fig. 4(a) indicates that the V camera can observe the entire cross section under investigation so the data acquired by all V camera detectors is used to reconstruct the emissivity function of the plasma radiation in one cross section. It can be seen that because of being obstructed the view field of the R camera, it cannot observe all the cross section under investigation and only a part of the image acquired by this camera is used to reconstruct the radiation emissivity function. In addition, Fig. 4(b) shows a visualization of the geometric matrix corresponding to the cameras layout depicted in 4(a) in the reconstruction plane. The obstruction of the R camera's field of view can negatively impact the tomography result and modification of the mount that would provide the solution to this problem is currently being planned for the future.

Furthermore, perspectives of implementing further data constraints in support of the cameras' data analyses e.g. linked to integration of other methods of light diagnostics is under consideration at present.

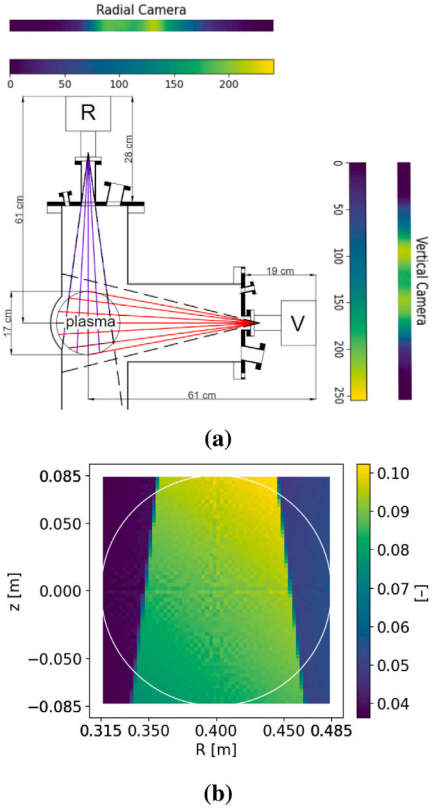

Fig. 4. (a) Schematic figure of the Poloidal cross-section of the GOLEM tokamak with the geometry of the lines of sight of two V and R fast visible cameras in respectively red and purple resulting in radial and vertical line integrated data. Example images captured by each camera are shown next to them, and (b) geometric matrix visualization in the reconstruction plane.

Table 1

The GOLEM tokamak - Discharge Database - #39304	
Minor radius	0.085 m
Major radius	0.4 m
Loop voltage (mean)	8 V
Plasma current (mean)	3 KA
Toroidal magnetic field (mean)	0.02 T
Discharge time duration	8.82 ms

5. Inversion reconstruction

This section presents a set of tomographic reconstructions from the data acquired by two R and V visible cameras viewing the GOLEM tokamak poloidal cross section described in Section 4 is presented. The tomographic inversion was performed by implementing the Tomotok package [21] based on Minimum Fisher Regularization (MFR) for the two-dimensional reconstruction.

The inversions were performed on a square rectilinear grid of size 60 × 60 pixels with a total size of 17 cm ×17 cm. The camera image spatial resolution = 1280 × 56 pixels corresponding to the Frame Rate = 40,000 fps was selected for the line integrated data recorded by two visible cameras.

Table 1 shows the tokamak and plasma parameters corresponding to the GOLEM tokamak - discharge Database - #39304. Fig. 5 shows the temporal evolution of the (a) Toroidal magnetic field, (b) Plasma current, and (c) Loop voltage of the selected plasma discharge depicting the discharge starts at $t = 4.07$ ms and ends at $t = 12.9$ ms.

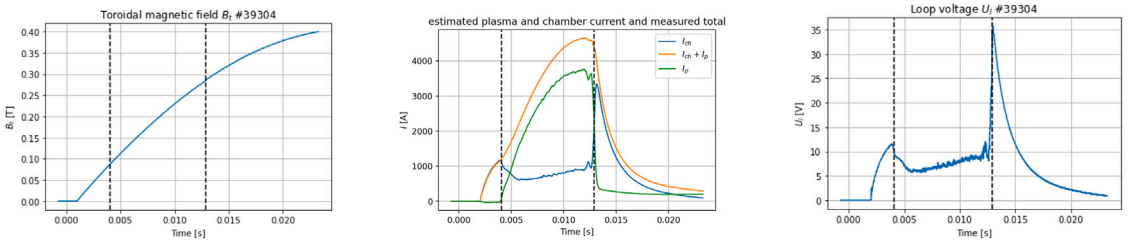

(a) (b) (c)

Fig. 5. Temporal evolution of the (a) Toroidal magnetic field, (b) Plasma current, and (c) Loop voltage of the plasma discharge.

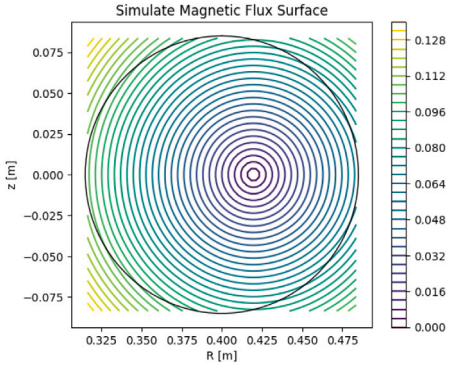

Fig. 6. The simulated magnetic flux surfaces in the tokamak cross section. Flux units are arbitrary.

In the present work, the smoothness of the result is enforced anisotropically in relation to the magnetic flux surfaces, so that smoothness along the surfaces is preferred to that across them. As the GOLEM tokamak is not equipped for the use of equilibrium reconstructions, the magnetic flux surfaces are only estimated as concentric circles in the tokamak cross section with a centre in the plasma centre [19]. In addition, an outward shift of the magnetic axis (the Shafranov shift) is considered due to the plasma pressure within the tokamak plasmas. Fig. 6 shows the contour plot of simulated magnetic flux surfaces in the tokamak cross section showing the concentric circular surfaces in the cross section with a centre shifted along r (tokamak radius) based on the approximated Shafranov shift. Deviations in the approximated magnetic flux surfaces from the real flux surfaces can be a source of systematic error in the reconstruction result. For example, the implementation of anisotropic smoothing in relation to the flux surfaces can result in more 'square' shape, rather than round that has been revealed in the phantom test.

Fig. 7 shows, the tomographic reconstruction of the line integrated data corresponding to the selected plasma discharge acquired by two visible cameras for four different time steps ($t_d = 0$ corresponds to the start of discharge.): (a) $t_d = 0.005$ ms, (b) $t_d = 1.13$ ms, (c) $t_d = 3.63$ ms, and (d) $t_d = 7.955$ ms. The white circle line marks the plasma edge as determined by the limiter.

Fig. 7(a) shows an emissivity profile concentrated in the centre of the chamber. This is an expected result, as it was reconstructed from the data from the very start of the discharge and so the plasma had not yet had time to reach a sufficiently high central temperature in order create a hollow visible light emissivity profile. The squaring of the circular profile visible in the phantom reconstruction can be seen here as well, which calls for further test for validation of tomography implementation and change in the limit in view mount in future work.

Fig. 7(b) shows the expected hollow profiles characteristic for visible light plasma emissivity. Only the edge plasma is usually cold enough to produce mostly visible light via bremsstrahlung and hydrogen light emissions. The reconstructed profile also displays a slight change between the areas visible by both cameras and the areas which are obstructed out of the view of the R camera. This is likely an artifact caused by the limited field of view of the R camera.

The squaring of the circular profile visible in the phantom reconstruction can be seen in Fig. 7(c) as well.

Fig. 7(d) shows a reconstruction from data acquired the end of the discharge. The profile is mostly concentrated to the very edge of the chamber, which can be explained by the interaction of the plasma with the limiter and the resulting higher concentration of radiating impurities. The higher emissivity in the top parts of chamber can be explained by the vertical displacement characteristic for the GOLEM tokamak, as described in [25]

The obstruction of the field of view of the R camera, as it was explained in Section 4, negatively influences the tomography results in several ways. Firstly, there is usually a clear divide between the areas of the reconstruction plane visible by both cameras and the areas outside of the view of the R camera. In addition, the tomography results can show a pronounced poloidal asymmetry due to the limited field of view.

Fig. 8 shows the line integrated signal acquired by two cameras and the backfitted signal corresponding to the inversion reconstructed result in Fig. 7(b) $t_d = 1.13$ ms in blue and red, respectively. The left and right part of the curve correspond to the data from the V and R cameras, respectively.

It can be easily seen that the hollow profiles retrieved from the reconstructed emissivity coincide with the position of hollow profiles corresponding to the line integrated data acquired by the two cameras. The variation of backfitted signal is similar to the line integrated signal, although backfitted signal corresponding to the V and R cameras shows respectively a reduction and increase in magnitude. It can be easily found from the figure that due to the obstruction of the view field of the R camera, the detector number of the R camera used for reconstruction is less than one of the V camera.

It is noteworthy that the asymmetric shape of the radiation distribution in the poloidal cross section can be explained as a consequence of inaccurate calibration of the cameras. For the next work, a relative calibration of the cameras' signal will be performed using a glow discharge to address this problem.

6. Conclusions and further planning

A selection of studies related to tomographic inversions using the newly installed fast cameras at the GOLEM tokamak are presented in this paper. A new diagnostic system consisting of two crossed (R and V) monochrome cameras Photron FASTCAM MINI UX50 with a Frame Rate of 40,000 fps (1280 × 56 pixels) in 12-bit ADC dynamic range with detector size = 10 μm × 10 μm was integrated into the GOLEM tokamak diagnostics. The tomographic inversions were performed on line integrated signal acquired by the two visible cameras. For that the Minimum Fisher Regularization (MFR) algorithm implementation from open source python package Tomotok [21] was used. The inversions were performed on a reconstruction grid of size 60 × 60 pixels. The smoothness of the result was enforced in relation to the magnetic flux surfaces. The results showed the expected hollow emissivity profile.

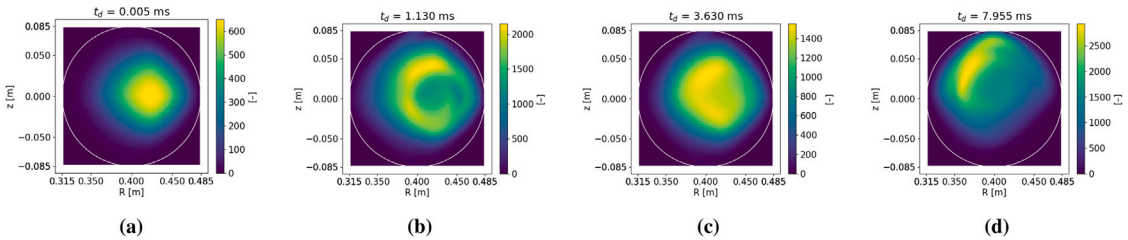

Fig. 7. Reconstruction Results of the plasma discharge for four different time steps ($t_d = 0$ corresponds to the start of discharge.): (a) $t_d = 0.005$ ms, (b) $t_d = 1.13$ ms, (c) $t_d = 3.63$ ms, and (d) $t_d = 7.955$ ms.

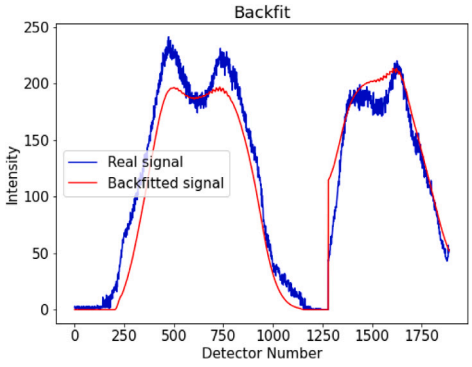

Fig. 8. Backfit test: The line integrated signal acquired by two cameras and the backfitted signal corresponding to the reconstructed result in Fig. 7(b), $t_d = 1.13$ ms in blue and red, respectively.

In order to test the accuracy of the result of the inversion reconstruction, a simple synthetic diagnostic model was used. Additionally, to demonstrate the accuracy of the reconstructed result, the backfitted signal corresponding to the reconstructed emissivity function was retrieved. The retrieved signal from the reconstructed emissivity function coincided in variation with the measured signal by two cameras but it showed a change in the magnitude of the intensity.

The phantom test and the reconstructed profile of the real data showed an overall more 'square' shape, rather than round which can be caused by the implemented anisotropic smoothing in the reconstruction, and consequently, the result calls for further test for validation of tomography implementation. In addition, the obstruction of the R camera's field of view can negatively impact the tomography result and modification of the mount that would provide the solution to this problem is currently being planned for the future. Furthermore, based on the error and accuracy of the present reconstruction result of the new installed visible cameras data, a relative calibration of the cameras on a glow discharge and possibly on another light source is needed to be considered. Finally, combination with richer light diagnostics e.g. spectroscopy, dedicated studies of fast transient phenomena, possibly in correlation with magnetic data, investigation of discharges with low impurity injection are the baselines for further planning.

Declaration of competing interest

This research has been supported from the Global Postdoc Fellowship Program of Czech Technical University in Prague and RVO 14000.

Data availability

The discharge data is available on the GOLEM wiki (http://golem.fjfi.cvut.cz/shots/39304/).

References

[1] T. Craciunescu, E. Peluso, A. Murari, M. Gelfusa, J. Contributors, Maximum likelihood bolometric tomography for the determination of the uncertainties in the radiation emission on JET TOKAMAK, Rev. Sci. Instrum. 89 (5) (2018) 053504.
[2] L. Ingesson, B. Alper, B. Peterson, J.C. Vallet, Chapter 7: Tomography diagnostics: Bolometry and soft-X-ray detection, Fusion Sci. Technol. 53 (2) (2008) 528–576.
[3] D. Zhang, R. Burhenn, C.D. Beidler, Y. Feng, H. Thomsen, C. Brandt, S. Buller, F. Reimold, P. Hacker, R. Laube, et al., Bolometer tomography on Wendelstein 7-X for study of radiation asymmetry, Nucl. Fusion 61 (11) (2021) 116043.
[4] A. Jardin, Soft X-ray measurements for impurity transport studies in tokamak plasmas (Ph.D. thesis), Aix-Marseille University, 2017.
[5] A. Jardin, J. Bielecki, D. Mazon, J. Dankowski, K. Król, Y. Peysson, M. Scholz, Neural networks: from image recognition to tokamak plasma tomography, Laser Particle Beams 37 (2) (2019) 171–175.
[6] P. Savrukhin, E. Shestakov, A study on the effects of magnetohydrodynamic perturbations on nonthermal beam formation during the current decay phase of disruptions in the T-10 tokamak, Nucl. Fusion 55 (4) (2015) 043016.
[7] F. Causa, M. Gospodarczyk, P. Buratti, D. Carnevale, R. De Angelis, B. Esposito, A. Grosso, G. Maddaluno, J.R. Martin-Solis, V. Piergotti, et al., Runaway electron imaging spectrometry (REIS) system, Rev. Sci. Instrum. 90 (7) (2019) 073501.
[8] J. Cerovsky, O. Ficker, V. Svoboda, E. Macusova, J. Mlynar, J. Caloud, V. Weinzettl, M. Hron, et al., Progress in HXR diagnostics at GOLEM and COMPASS tokamaks, J. Instrum. 17 (01) (2022) C01033.
[9] D. Zhang, R. Burhenn, R. Koenig, L. Giannone, P. Grodzki, B. Klein, K. Grosser, J. Baldzuhn, K. Ewert, V. Erckmann, et al., Design criteria of the bolometer diagnostic for steady-state operation of the W7-X stellarator, Rev. Sci. Instrum. 81 (10) (2010) 10E134.
[10] F. Matos, J. Svensson, A. Pavone, T. Odstrčil, F. Jenko, Deep learning for Gaussian process soft X-ray tomography model selection in the ASDEX upgrade tokamak, Rev. Sci. Instrum. 91 (10) (2020) 103501.
[11] J. Svoboda, M. Imrisek, K. Mikszuta-Michalik, J. Mlynar, O. Ficker, P. Bilkova, V. Weinzettl, F. Jaulmes, M. Hron, R. Panek, Conceptual design of tomographic soft X-ray detectors for COMPASS-U tokamak, Fusion Eng. Des. 168 (2021) 112656.
[12] J. Mlynar, M. Tomes, M. Imrisek, B. Alper, M. O'Mullane, T. Odstrcil, T. Puetterich, et al., Soft X-ray tomographic reconstruction of JET ILW plasmas with tungsten impurity and different spectral response of detectors, Fusion Eng. Des. 96 (2015) 869–872.
[13] A. Sperduti, M. Cecconello, S. Conroy, J. Eriksson, K. Kirov, L. Giacomelli, J. Contributors, Plasma position measurement with collimated neutron flux monitor diagnostics on JET, Fusion Eng. Des. 168 (2021) 112597.
[14] K. Mikszuta-Michalik, M. Imrisek, B. Esposito, D. Marocco, J. Mlynar, O. Ficker, A total neutron yield constraint implemented to the RNC emissivity reconstruction on ITER tokamak, Fusion Eng. Des. 160 (2020) 111840.
[15] M. Odstrčil, J. Mlynář, V. Weinzettl, P. Háček, T. Odstrčil, G. Verdoolaege, M. Berta, T. Szabolics, A. Bencze, Plasma tomographic reconstruction from tangentially viewing camera with background subtraction, Rev. Sci. Instrum. 85 (1) (2014) 013509.
[16] T. Odstrčil, T. Pütterich, M. Odstrčil, A. Gude, V. Igochine, U. Stroth, A.U. Team, Optimized tomography methods for plasma emissivity reconstruction at the ASDEX upgrade tokamak, Rev. Sci. Instrum. 87 (12) (2016) 123505.
[17] J. Brotánková, Study of high temperature plasma in tokamak-like experimental devices, 2009.
[18] J. Mlynar, V. Weinzettl, G. Bonheure, A. Murari, J.E. CONTRIBUTORS, Inversion techniques in the soft-X-ray tomography of fusion plasmas: toward real-time applications, Fusion Sci. Technol. 58 (3) (2010) 733–741.
[19] J. Mlynar, T. Craciunescu, D.R. Ferreira, P. Carvalho, O. Ficker, O. Grover, M. Imrisek, J. Svoboda, Current research into applications of tomography for fusion diagnostics, J. Fusion Energy 38 (3) (2019) 458–466.
[20] C. Groetsch, The Theory of Tikhonov Regularization for Fredholm Equations, Boston Pitman Publication, 1984, p. 104.
[21] J. Svoboda, J. Cavalier, O. Ficker, M. Imríšek, J. Mlynář, M. Hron, Tomotok: python package for tomography of tokamak plasma radiation, J. Instrum. 16 (12) (2021) C12015.

[22] J. Mlynar, M. Imrisek, V. Weinzettl, M. Odstrcil, J. Havlicek, F. Janky, B. Alper, A. Murari, J.E. Contributors, Introducing minimum Fisher regularisation tomography to AXUV and soft x-ray diagnostic systems of the COMPASS tokamak, Rev. Sci. Instrum. 83 (10) (2012) 10E531.

[23] V. Svoboda, M. Zhekova, M. Dimitrova, P. Marinova, A. Podolník, J. Stockel, Operational domain in hydrogen plasmas on the GOLEM tokamak, J. Fusion Energy 38 (2) (2019) 253–261.

[24] Photron Europe Limited, Product datasheet mini UX fastcam series by photron, 2021, URL: http://photron.com/wp-content/uploads/2015/11/Mini-UX-REV16.9.29.pdf.

[25] G. Sarancha, A. Drozd, S. Ganin, D. Kropachkova, I. Kudashev, V. Kulagin, M. Lauerova, A. Melnikov, N. Sergeev, O. Krokhalev, et al., Hydrogen and helium plasmas in the GOLEM tokamak.